CHEMISTRY OF MATERIALS

ARTICLE

pubs.acs.org/cm

Facile Synthesis of Transparent Mesostructured Composites and Corresponding Crack-free Mesoporous Carbon/Silica Monoliths

Hao Wei, Yingying Lv, Lu Han, Bo Tu,* and Dongyuan Zhao*

Department of Chemistry, Shanghai Key Laboratory of Molecular Catalysis and Innovative Materials, Laboratory of Advanced Materials, Fudan University, Shanghai 200433, China

Supporting Information

ABSTRACT: Transparent ordered mesostructured resin-silica composite monoliths with uniform rectangular shape which fully copies the inner-shape of vessels and size (5 × 3 × 0.3 cm^3) are prepared via a facile approach of evaporation induced self-assembly (EISA) without adding any protecting agent by using triblock copolymer Pluronic F127 as a template. Ordered mesoporous carbon-silica composite monoliths can be obtained in a wide range of silica content (34−82 wt %) after calcination in N_2. Monolithic shape can be maintained with shrinkage (~20%) in sizes. Furthermore, each component of the composites can be easily removed after the simple post treatments. After etching silica, mesoporous carbon monoliths retain the same in shape and sizes, but show much larger pore volume (~2.65 cm^3/g) and higher surface area (~1800 m^2/g) than the carbon−silica composites. Besides, mesoporous silica monoliths with large pore size (~14.6 nm) show an integral and uniform shape after air combustion. The obtained mesoporous carbon monoliths show high capacitance (186 F/g) and high cycling stability (8% capacitance loss after 1000 cycles), exhibiting an excellent potential in capacitor applications.

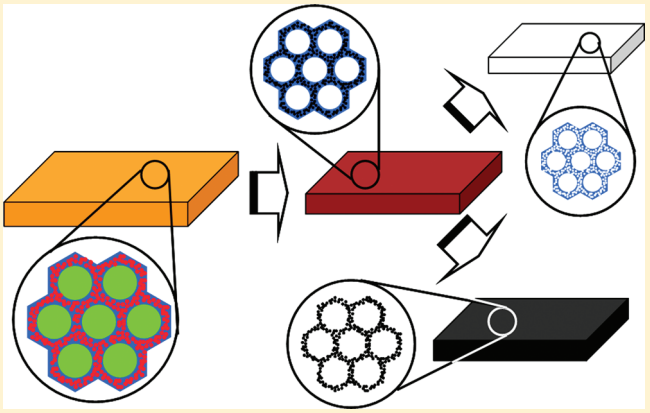

KEYWORDS: mesoporous, carbon, crack-free, monolith, composite, electrochemistry

1. INTRODUCTION

Over the past two decades, ordered mesoporous silica materials have attracted great interest in many fields such as catalysis, separation, and drug delivery,[1,2] because of their variable structure and relatively large pore size. Mesoporous silica materials with various morphologies have been obtained, such as thin films,[3,4] microspheres,[5,6] single crystals,[7] fibers,[8] and monoliths.[9−12] It is widely accepted that mesoporous silica monoliths with large pore sizes show great potential in optical devices, such as sensors and nonlinear optical media.[13] Moreover, mesoporous monolithic materials can provide a fast mass transportation compared with powders,[11,14] because the bulk size can be removed easily from solutions after separation. Mesoporous silica monoliths have been prepared by evaporating solution in gel,[15] fusion of spheres,[16] coating suitable precursors into/onto polyurethane foams,[17] and immersing what within colloidal liquid templates.[18]

However, the main problem of preparing crack-free mesoporous silica monoliths is the occurrence of macro-flaws in the solvent removal process, because of internal pressure gradient caused by large shrinkage of the gel. To date, some methods were introduced to overcome this drawback on the basis of the sol−gel process,[19] such as critical point extraction[20] and vacuum drying.[21] Yang et al. developed a fast way to prepare transparent mesostructured composite monoliths by covering a paraffin layer during the solution evaporation process.[22] The protecting layer changes the alcohol−vapor interface to alcohol−paraffin, which leads to elimination of macro-cracks during fast evaporation process. As a result, transparent composite monoliths can be easily obtained. However, this procedure is complicated and calcined mesoporous silica monoliths still have many internal and external macro-cracks. The pore size is small (~5.65 nm) because of large shrinkage of the monoliths in the calcination process (15−20%) without hydrothermal treatment, which may limit the applications in macromolecular separation. Xue and co-workers developed another method to prepare transparent mesoporous silica monoliths.[23] The macro-cracks are prevented by replacing methanol solvent with water during the evaporation. Ethylene glycol and functional organic silanes were used as a pore directing agent and a precursor, respectively. As a result, disordered mesoporous silica monoliths were obtained.

In recent years, ordered mesoporous carbon materials are considered as the most promising materials for the supercapacitor application due to their large accessible surface areas, narrow pore size distribution, and stable physicochemical properties.[1,24] On the basis of preparing silica monoliths, synthesis of mesoporous

Received: January 4, 2011
Revised: April 2, 2011
Published: April 15, 2011

carbon monoliths also receives much attention for their potential in catalysis substrates, electrodes, and adsorbents. The common approach to prepare ordered mesoporous carbonaceous monoliths is the nanocasting strategy, which is complicated and costly.[25−27] Huang and co-workers introduced a hydrothermal synthesis of the ordered mesoporous carbon monoliths in cylindrical shape, but their surface areas (∼360 m^2/g) and pore volume (∼0.36 cm^3/g) are quite low due to the shrinkage of frameworks during the pyrolysis.[28] Until now, the facile synthesis of transparent mesostructured composites and corresponding crack-free mesoporous carbon/silica monoliths still remains a big challenge. Recently, a triconstituent coassembly strategy has been developed to synthesize ordered mesoporous polymer-silica and carbon-silica composites.[29] The polymer and silica species interpenetrate and sustain each other in the composite frameworks. After a simple post treatment, ordered mesoporous either carbon or silica materials with large pore sizes can be obtained. Because the ordered mesoporous composites can be obtained in a wide range of silica contents, this triconstituent coassembly strategy would be suitable for the simultaneous synthesis of ordered mesoporous carbon/silica monoliths, in which the introduction of polymers can reduce macro-cracks during the solvent evaporation.

In this paper, we demonstrate a facile approach to synthesize ordered mesostructured composite monoliths, wherein triblock copolymer F127 is used as a template, soluble resol polymer as an organic precursor, TEOS as a silica precursor. Monoliths with rectangular shapes can be prepared via the triconstituent coassembly strategy through an evaporation induced self-assembly (EISA) without adding any protecting agent, The transparent monoliths fully replicate the inner-shape and size ($5 \times 3 \times 0.3$ cm^3) of the adopted vessels, which can be easily variable. Ordered mesoporous carbon-silica composite monoliths can be obtained in a wide range of silica contents (34−82 wt %) after pyrolysis in N_2 at 600 °C. The shape can be maintained with a volume shrinkage (∼20%). After the removal of silica by HF etching or carbon by a simple combustion in air, ordered mesoporous carbon or silica monoliths can be obtained from a single original composite, respectively. Mesoporous carbon monoliths retain the same shape and size and show much large pore volume (∼2.65 cm^3/g) and high surface area (∼1800 m^2/g). Simultaneously, the obtained mesoporous silica monoliths show large pore size (∼14.6 nm) and an integral shape. In addition, the mesoporous carbon show a high capacitance and cyclic stability in electrochemical double layer capacitor (EDLC).

2. EXPERIMENTAL SECTION

2.1. Chemicals. Poly(ethylene oxide)-*block*-poly(propylene oxide)-*block*-poly (ethylene oxide) triblock copolymer Pluronic F127 (M_w = 12 600, $PEO_{106}PPO_{70}PEO_{106}$) was purchased from Acros Corp. Tetraethyl orthosilicate (TEOS), phenol, formalin solution (37 wt %), NaOH, HCl, and ethanol were purchased from Shanghai Chemical Corp. All chemicals were used as received without any further purification.

2.2. Preparation of Resol Precursors. The 20 wt % of phenolic resol solution was prepared according to the previous report.[30] In a typical procedure, 0.61 g of phenol was melted at 40 °C in a flask and mixed with 0.13 g of 20 wt % NaOH aqueous solution under stirring. After 10 min, 1.05 g of formalin (37 wt % formaldehyde) was added and keep on stirring at 75 °C for 1 h. The mixture was cooled down to room temperature and the pH value was adjusted to neutral (∼7.0). The final product was dissolved in ethanol (20 wt %) after rotatory evaporation at 50 °C under a vacuum to remove water.

2.3. Synthesis of Mesostructured Polymer−Silica and Carbon−Silica Monoliths. Transparent mesostructured polymer-silica monoliths were prepared by coassembly of resol, TEOS and triblock copolymer F127 via a modified EISA method. In a typical procedure, 3.2 g of F127 was dissolved in 12 mL of ethanol with 1.0 g of 0.2 M HCl and stirred for 2 h at 40 °C. Then, 4.0 g of TEOS and 6.0 g of 20 wt % resol solution were added under stirring to obtain a clear solution. The mixture was transferred into vessels (rectangular shape with an inner volume of $5 \times 3 \times 3$ cm^3) and the solvent was evaporated for 72 h at room temperature. These pieces were heated in an oven at 50 °C for another 72 h. The as-made mesostructured polymer−silica monoliths were marked as PSM-61. PSM-*x* denotes the polymer-silica monoliths, wherein *x* represents the silica content. Pyrolysis was carried out in a tubular furnace at 600 °C for 3 h under a N_2 flow with a heating rate of 0.3 °C/min, and the obtained mesoporous carbon-silica monoliths were marked as CSM-61. "CSM-*x*" denotes the carbon−silica monoliths, wherein *x* represents the silica content.

2.4. Synthesis of Mesoporous Carbon and Silica Monoliths. The silica was removed by immersing the mesoporous carbon−silica composite monoliths in 10 wt % HF aqueous solution at room temperature for 24 h, followed by washing with water. Mesoporous carbon monoliths were obtained after drying for overnight. Mesoporous silica monoliths were obtained by calcination at 550 °C for 5 h in air. The mesoporous carbon and silica monoliths were marked as CM-*x* and SM-*x*, respectively, wherein *x* represents the silica content of the corresponding carbon/silica monoliths.

2.5. Characterization. The small-angle X-ray scattering (SAXS) measurements were taken on a Nanostar U small-angle X-ray scattering system (Bruker, Germany) using Cu Kα radiation (40 kV, 35 mA). Nitrogen sorption isotherms were measured at 77 K with a Micromeritics Tristar 3000 analyzer (USA). Before measurements, the samples were degassed in a vacuum for at least 6 h at 180 °C. The specific surface areas were calculated by using the Brunauer−Emmett−Teller (BET) method. The pore size distributions were derived from the adsorption branches of isotherms by using the Barrett−Joyner−Halenda (BJH) model. The total pore volumes were estimated from the adsorbed amount at a relative pressure P/P_0 of 0.992. Transmission electron microscopy (TEM) experiments were conducted on a JEOL 2100F microscope (Japan) operated at 200 kV. The samples were crushed into powder and dispersed in ethanol before analysis. High-resolution scanning electron microscopy (HRSEM) images of the samples were taken using a Hitachi S-4800 ultrahigh resolution cold FEG (Japan) with an in-lens electron optic operating at 20 kV.

2.6. Electrochemical Measurements. Cyclic voltammetry and galvanostatic charge/discharge cycling of the mesoporous carbon powders were employed in the evaluation of electrochemical behaviors by using the electrochemical analyzer, CHI 606B electrochemical analyzer system under ambient condition. 6.0 M of KOH solution was used as the electrolyte. The capacitance behaviors were measured by cyclic voltammetry and charge−discharge tests using a three-electrode glass cell in which Pt foil was used as the counter electrode, and a Hg/HgO electrode (0.052 V vs. the normal hydrogen electrode, NHE) as the reference electrode. Cyclic performance tests were performed in 6.0 M of KOH aqueous electrolyte by charge−discharge cycling at current density of 1.0 A/g, using a Land CT2001A Battery Cycler (Wuhan, China).

3. RESULTS AND DISCUSSION

3.1. Crack-free Mesoporous Monoliths. The crack-free mesostructured polymer−silica monoliths can be prepared by using phenolic resol as an organic precursor, TEOS as a silica precursor and triblock copolymer F127 as a template via a

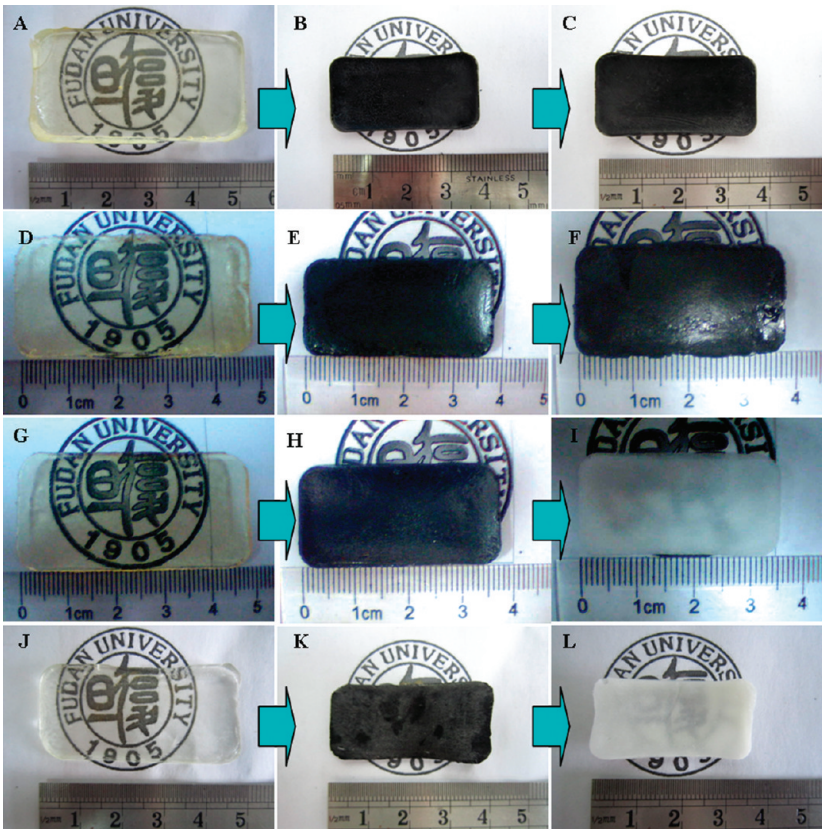

Figure 1. Optical photos of the (A−D) polymer−silica monoliths, (E−H) carbon−silica monoliths, (I, J) carbon monoliths, and (K, L) silica monoliths with different silica contents (weight percentages) of (E) 36, (F, G) 61, and (H) 82%, respectively.

prolonged EISA method. The optical images show that the as-made mesostructured polymer-silica composite monoliths (Figure 1A−D) with different silica contents are integral and transparent, which faithfully replicate the shape of vessels. The size of all the polymer-silica composite monoliths is similar in 5 × 3 × 0.3 cm^3. The shape and size of the monoliths can be easily varied by using different vessels and changing amount of the reactants. The color of the as-made monoliths is yellow (Figure 1A), then changes to colorless as silica percentage increases (Figure 1D), which is ascribed to the natural color of the resol and silica. The mesoporous carbon-silica composite monoliths (Figure 1E−H) obtained after pyrolysis at 600 °C for 3 h under N_2 exhibit dark brown color, and integral macroscopic morphology is still retained satisfactorily with an even shrinkage of 26% (Figure 1E), which decreases slightly to 20% as increasing silica percentage (Figure 1H). It is attributed to the high stability of silica frameworks during the pyrolysis. After etching of the silica component by HF solution, the size of the mesoporous carbon monoliths (Figure 1I, J) remains the same as that of the mesoporous composites because of the mild etching condition at room temperature. The carbon monoliths (CM-34) derived from a low silica content (34%) show unchanged morphology after the silica etching (Figure 1I). By contrast, the sample with a high silica content (CM-61) is very fragile, and many defects can be observed on the surface (Figure 1J), which are a result of the partial collapse of the carbon frameworks after large amount silica etching. Extremely, integral carbon monoliths are not obtained in the sample CM-82 with the highest silica content (82%), indicating that few carbonaceous residues can not self-sustain without silica framework. After the combustion at 550 °C for 6 h in air, the crack-free silica monoliths with white color and integral shape

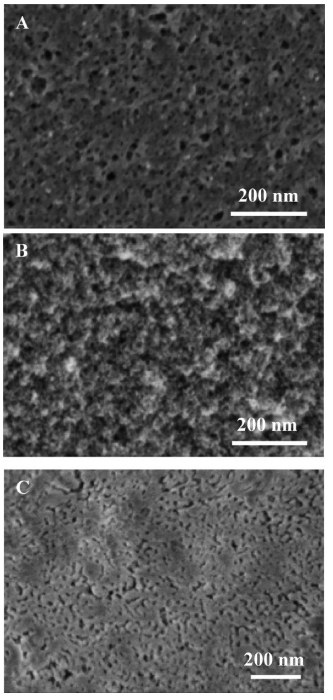

Figure 2. Top-view SEM images of the mesoporous monoliths: (A) the carbon−silica CSM-61, (B) the carbon CM-61 and (C) the silica SM-61.

dx.doi.org/10.1021/cm2000182 |*Chem. Mater.* 2011, 23, 2353–2360

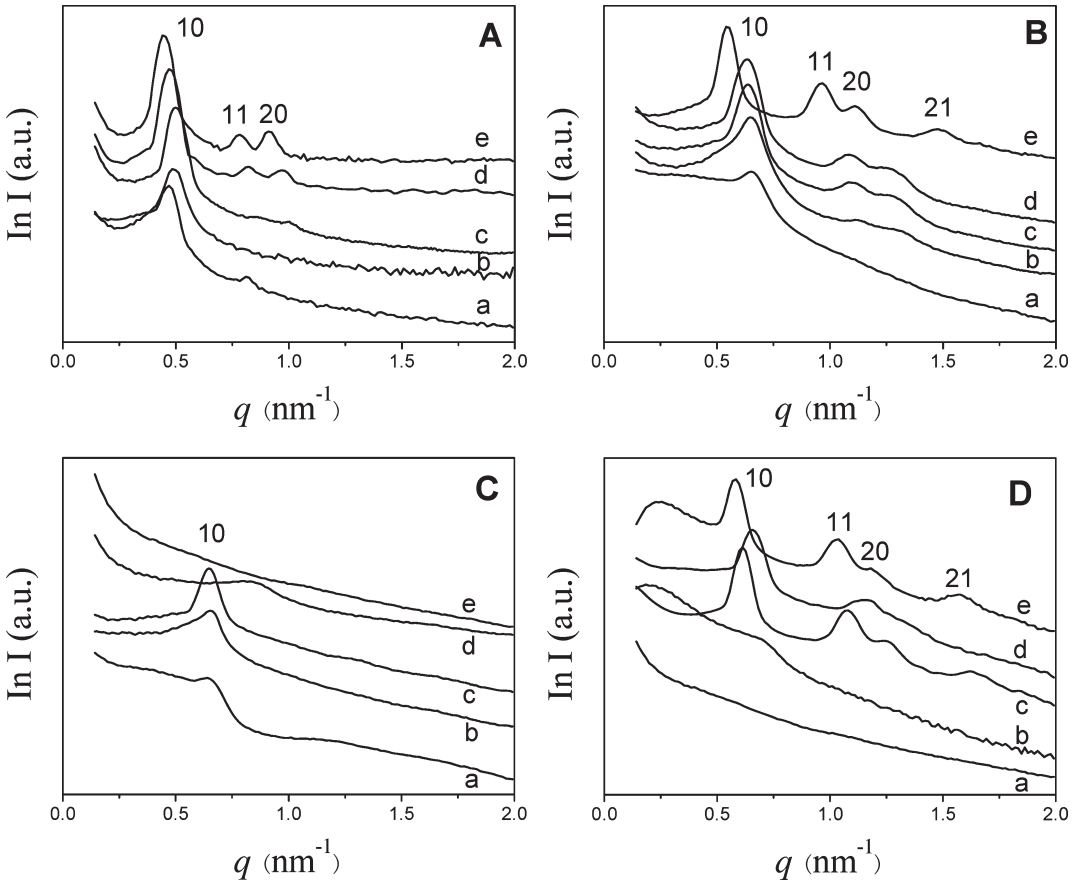

Figure 3. SAXS patterns of (A) the as-made mesostructured polymer−silica monoliths, (B) the mesoporous carbon−silica composite monoliths, (C) the corresponding carbon monoliths after etching silica by HF and (D) silica monoliths after burning out carbon at 500 °C in air, with different silica contents. In A: (a) PSM-34, (b) PSM-52, (c) PSM-61, (d) PSM-70, and (e) PSM-82. In B: (a) CSM-34, (b) CSM-52, (c) CSM-61, (d) CSM-70, and (e) CSM-82. In C: (a) CM-34, (b) CM-52, (c) CM-61, (d) CM-70, and (e) CM-82. In D: (a) SM-34, (b) SM-52, (c) SM-61, (d) SM-70, and (e) SM-82.

show a further 5% volume shrinkage and lose transparency (Figure 1K, L), which is caused by further cross-linking of the silicate frameworks at the high temperature. Similar to the carbon monoliths, no integral silica monoliths can be obtained in the case with the lowest silica content (34%).

SEM images show that the surface of the mesoporous carbon-silica composite monoliths is smooth and no cracking in any domain (Figure 2A). The mesoporosity on the surface with a wide distribution from 5 to 35 nm in large domains is observed. After etching silica, the mesoporous carbon monoliths (Figure 2B) also show no-cracking domain. Many large mesopores packed with nanoparticles make the carbonaceous surface much coarser, suggesting an open and accessible mesopore channels, resulting from an inhomogeneous distribution of silica and carbon components on the surface due to the fast evaporation of solvent during the assembly process. The wider pore distribution (5−50 nm) on the surface should provide open pathways in the fast mass transformation. On the contrary, the surface of the mesoporous silica monoliths (Figure 2C) after burning out the carbon component is relatively smooth, which is similar to that of the carbon−silica composites. The surface structure seems to be smoother and more compact because of further shrinkage of the mesostructure during the air combustion.

SAXS pattern of the mesostructured polymer-silica composite monoliths with a high silica content of 82% (Figure 3Ae, PSM-82) reveals three well-resolved scattering peaks, which can be indexed to 10, 11, 20 reflection of two-dimensional (2D) hexagonal symmetry (*p6m*), indicating a highly ordered mesostructure. As the silica content decreases, only one scattering peak is observed, suggesting that the regularity of the mesostructure a little degrades. When the silica content decreases to 61%, the unit-cell parameter of the polymer-silica monoliths has a minimum of 14.6 nm (Table 1). After pyrolysis in N_2 at 600 °C, the corresponding mesoporous carbon−silica composite monoliths (CSM-82) exhibit four resolved SAXS patterns of highly ordered 2D hexagonal symmetry (Figure 3Be). SAXS patterns (Figure 3B) become poorly resolved to only one weak scattering peak for the 10 reflection as the silica content decreasing. Relative to that of the as-prepared samples, the unit-cell parameters of the mesoporous carbon-silica monoliths reduce from 18.3 to 32.4% as the silica content increases (Table 1), which are coincident approximately with the macroscopical shrinkage calculated from the optical images (Figure 1), and the lowest shrinkage of CSM-82 confirms a rigid interpenetration of the silica and resin polymer frameworks.

After etching silica frameworks, ordered mesostructure is still retained in all mesoporous carbon monoliths (Figure 3C). The lack of the scattering peaks in high silica content (the sample CM-61) should be ascribed to low contrast of the incompact carbon walls without the silica. A dramatic change of unit cell parameter (Figure 3C) from 11.5 to 8.71 nm (Table 1) is observed with high silica content, indicating the partial collapse

dx.doi.org/10.1021/cm2000182 |*Chem. Mater.* 2011, 23, 2353–2360

Table 1. Physicochemical Properties of the Mesoporous Carbon−Silica Composite, Carbon and Silica Monoliths with Different Silica Content[a]

sample name	a_0 (nm)	S_{BET} (m^2/g)	D (nm)	V (cm^3/g)	shrinkage (%)
PSM-34	16.4				
CSM-34	11.1	476	6.8	0.66	32.4
CM-34	11.3	1650	7.7	1.63	
SM-34		234	10.4	0.83	
PSM-52	15.4				
CSM-52	11.2	462	6.1	0.56	27.3
CM-52	11.1	1560	6.0	1.65	
SM-52	10.5	306	14.6	1.13	31.8
PSM-61	14.6				
CSM-61	11.3	459	6.7	0.64	22.6
CM-61	11.9	1800	7.5	2.65	
SM-61	10.5	441	9.5	1.09	28.1
PSM-70	15.0				
CSM-70	11.5	450	7.7	0.61	23.3
CM-70	8.71	1700	/	1.22	
SM-70	11.1	392	9.4	0.96	26.0
PSM-82	16.4				
CSM-82	13.4	492	10.4	0.96	18.3
CM-82		693		0.40	
SM-82	12.4	359	12.3	1.02	24.4

[a] a_0, the unit-cell parameter, is calculated by using the formula $a_0 = 2d/\sqrt{3}$, S_{BET} is the BET surface area. D is the pore size diameter. V is the pore volume.

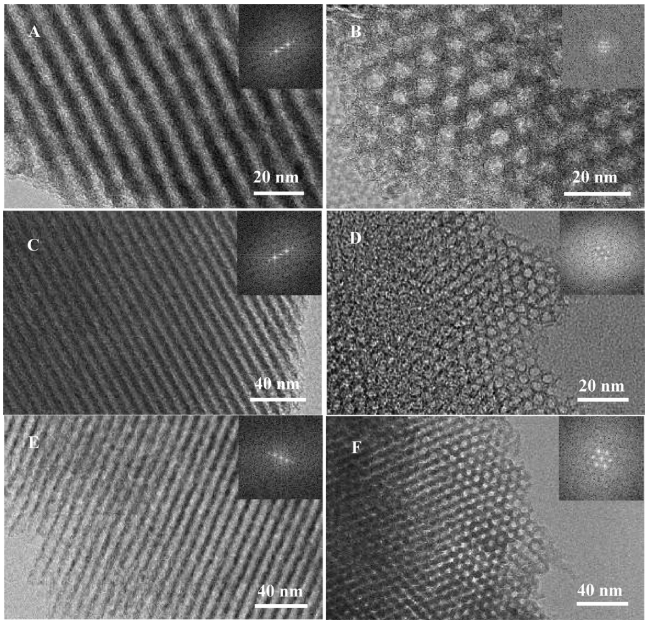

Figure 4. TEM images of the mesoporous monoliths: (A, B) the carbon−silica CSM-61, (C, D) the carbon CM-61, and (E, F) the silica SM-61, viewed from the (A, C, E) [110] and (B, D, F) [001] directions. The insets are the corresponding FFT.

of carbon framework derived from etching major contents in the frameworks. After burning out carbon content from the frameworks, the SAXS patterns of mesoporous silica monoliths with high silica contents (in the case of the samples SM-82, SM-70 and SM-61) show four well-resolved scattering peaks (Figure 3D), revealing a highly ordered 2-D hexagonal mesostructure. Although no SAXS pattern is observed in the cases of the samples (SM-52, SM-34) with a low silica content (Figure 3Da,b), suggesting that the silica frameworks completely collapse during the combustion of large amount of carbon. Furthermore, the shrinkages of the silica frameworks increase to 31.8% after combusting carbonaceous components.

TEM images further confirm that the mesoporous carbon−silica composite, carbon, and silica monoliths can be prepared by using the coassembly approach after removal of the carbon and silica contents, respectively. Here, we take the representative samples with the silica content of 61% as an example for the demonstration. TEM images of the mesoporous carbon−silica composite monoliths (CSM-61) show large domains of highly ordered mesostructure (Figure 4A, B), which are attributed to the [110] and [001] directions of 2-D hexagonal symmetry (*p6m*). The unit cell parameter of the mesoporous composite monolith measured from the TEM images (∼ 11.2 nm) is well in agreement with that from the SAXS patterns. The TEM image of the mesoporous carbon monoliths (CM-61) shows some small mesopores penetrated onto the pore walls (Figure 4C,D), which is resulted from the removal of silica component. The unit-cell parameter of the mesoporous carbon monolith measured from the TEM images is about 11 nm, which is also in agreement with that from SAXS data. After the air combustion at 500 °C to remove the carbon component, the obtained mesoporous silica monoliths (SM-61) show also ordered hexagonal mesostructure with much condensed frameworks (Figure 4E,F), implying further polymerization and cross-linking of silicate species in the pore walls. The unit cell parameter measured from TEM images (∼10 nm) is similar with that for the mesoporous silica, further suggesting a uniform shrinkage of the framework.

N_2 sorption isotherms were measured for the mesoporous carbon-silica, carbon and silica monoliths to evaluate their textural properties and shown in Figure S1 in the Supporting Information. The mesoporous carbon-silica composite monoliths with high silica content (e.g., CSM-82) exhibit type-IV curve with a sharp capillary condensation step and an H1-type hysteresis loop (see Figure S1A in the Supporting Information), which is typical of ordered mesoporous materials with cylindrical channels. Moreover, the pore sizes increase from 6.8 to 10.4 nm as the silica content increases (see Figure S1B in the Supporting Information), relating to the rigid nature of the silica networks. Differently, the N_2 sorption isotherms of the mesoporous carbon monoliths show an H2-type hysteresis loop (see Figure S1C in the Supporting Information), suggesting imperfect cylinder channels, which should be related to large voids caused by the silica etching. Remarkably, the sample with silica content of 61 wt % exhibits the best textural parameters of ∼1800 m^2/g in surface area and 2.65 cm^3/g in pore volume (Table 1). And this carbon monolith has an obvious bimodal mesopore size distribution at the mean value of 7.5 and 3 nm (see Figure S1Dc in the Supporting Information), which are respective to the primary mesopore contributed from the triblock copolymer F127 template and the secondary mesopore ascribed to the voids on the pore walls. The mesoporous silica monolith (SM-52) shows representative type-IV curve with perfect H1-type hysteresis loop (see Figure S1E in the Supporting Information), clearly indicating regular cylindrical mesopore channels. Pore size is as large as 14.6 nm with a wide distribution (see Figure S1Fb in the

Scheme 1. Formation Process of the Mesostructured Composite Monoliths and Corresponding Mesoporous Carbon and Silica Monoliths

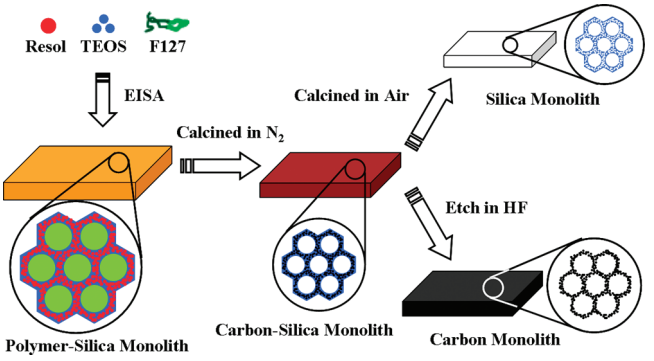

Supporting Information), which is much larger than its unit-cell parameter (~10.5 nm) (Table 1), implying interpenetrated mesopore channels. As the silica content increases, the mesopore size decreases a little (Figure S1F), excepting a dramatically large mesopore (12.3 nm). The BET surface area exhibits a maximum of 441 m^2/g with a silica content of 61%. Moreover, the mesoporous silica monoliths with the content of 52 and 61% show larger pore volume, which are 1.13 and 1.09 cm^3/g, respectively. The result implies that the well closed interpenetration of the silica and resin polymer frameworks could make stable mesostructured frameworks.[31]

On the basis of the above observation, the formation process of the crack-free mesoporous monoliths is shown in Scheme 1. During the EISA process, triconstituent coassembly of phenolic resols, silicate oligomers hydrolyzed from TEOS and Pluronic F127 can take place, and the highly ordered mesostructure is formed. Because both phenolic resols and silicate oligomers can interact with hydrophilic segment (PEO) of Pluronic F127 templates by hydrogen-bonding, the organic polymers interpenetrate with inorganic silicate oligomers to form highly dispersing composite frameworks.[29] Althouh the evaporating rate is relatively high and the composite gel loses its permeability, an internal pressure gradient[32] is built up inside the gel, which normally leads to cracking from flaws at the interface in the conventional preparation of the silica monoliths. However, in our case, by introducing organic polymeric resol precursors into the gel, macro-cracks caused by the pressure gradient could be reduced because of their plasticity. In addition, the existence of the resin polymers in the interpenetrating frameworks could make the composite gels more flexible, which endures large shrinkage during the heating treatment to remove the templates. Furthermore, cross-linked silica network in the mesostructure is much more rigid than carbon and can sustain the composite framework, shrinkage of the macroscopical size is reduced during the pyrolysis at high temperature. The synergic effect of the flexible polymeric components and rigid silica networks can result in homogeneous shrinkage and eliminate the macro-crack on surface. Therefore, the transparent mesostructured polymer–silica and crack-free mesoporous carbon–silica composite monoliths are obtained without any additional protecting layer. When the carbon content in the composites is enough high, the morphology of the mesoporous carbon monoliths is retained after etching silica components at room temperature by HF. Because of the carbon combustion in air with a slow heating rate

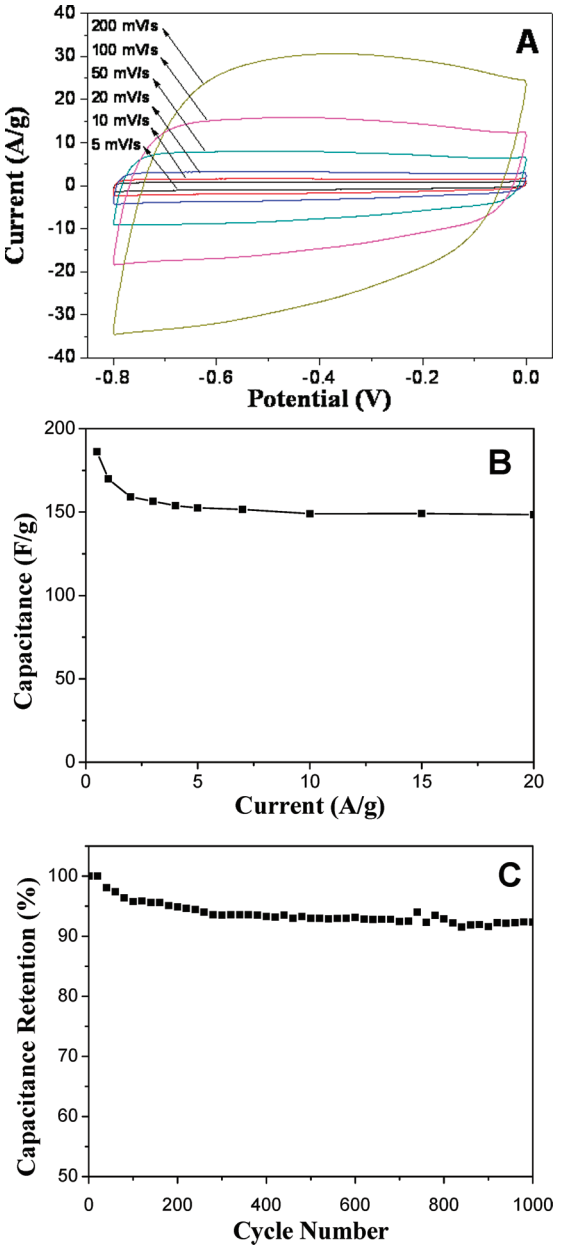

Figure 5. Electrochemical performances of the mesoporous carbon monoliths (CM-61). (A) Cyclic voltammetry curves at different scan rates; (B) capacitance as a function of different current density; (C) cycle performance at a current density of 1.0 A/g.

(0.3 °C/min), the residual silica frameworks could endure slight further shrinkage (~5%) and the ordered mesoporous silica monoliths retain integral and crack-free shape. In this process, large amounts of the secondary mesopores with a wide size distribution are yielded on the pore walls, which results in 3D interconnected mesopore channels. Compared with the preparations reported previously,[25,33] our process without adding any protecting agent is simple and reproduciable and can be used to synthesize transparent mesostructured composite monoliths, and crack-free silica and carbon monoliths with a large pore size, high surface area, and pore volume simultaneously.

3.2. Electrochemical Performance of Mesoporous Carbon Monoliths. The electrochemical performances of the

mesoporous carbon monoliths (take the sample CM-61 as an example) with the large surface area and bimodal pore size distribution were measured by using cyclic voltammetry (CV) and galvanostatic charge/discharge method (Figure 5A). At the scan rate of 5 mV/s, the CV profiles of the sample show a standard rectangular shape (see Figure S2 in the Supporting Information), clearly indicating good capacitive behavior at the low drain rate. The CV profiles at a high scan rate of 200 mV/s still maintain a quasi-rectangular shape with only slight distortion (Figure 5A), which shows that the sample possesses excellent capacitive behavior at high drain rate, suggesting that the hierarchical porous structure favors the fast ionic transportation within the mesopores and short diffusion distance.

The galvanostatic charge/discharge profiles of the sample (CM-61) with different current densities from 0.5 to 20 A/g (see Figure S3 in the Supporting Information) show isosceles triangle curves, suggesting the simulative capacitor with good electrochemical stability and reversibility. From the gradual voltage change (V) (Figure 5B), the corresponding specific capacitance can be calculated by the equation:[34] $C = It/mU$, where I is the discharge current (mA), t is the total discharge time (s), m is the total mass of active material in both electrodes (g), U is the potential difference during the discharging (V), and C is single-electrode capacitance (F/g), respectively. When the current density increases from 0.5 to 20 A/g, the capacitance is about 149 F/g, which is approximately 80% of the data (186 F/g) calculated at 0.5 A/g (Figure 5B). This indicates that the high capacitance at a low current density is resulted from enough diffusion time of the ions from mesopores to micropores. At a high current density, the hydrated ions can only partially penetrate into the small mesopores because of the steric hindrance of the small pores and time limitation of the fast charge/discharge process.[35] As a result of the silica etching, mesopores of the carbon monolith in different sizes and locations make large percentage of the surface area accessible which benefits for the EDLC performance. The capacitances drop slowly (~6%) as the current density increases from 2 to 20 A/g (Figure 5B), suggesting a good rate capability of CM-61. The capacitance retention of the sample CM-61 remains 92% (Figure 5C) after 1000 consecutive cycles, indicating a long-term electrochemical stability.

4. CONCLUSION

Highly ordered mesostructured polymer−silica monoliths with transparent and crack-free shape have been prepared by using the resol and TEOS as the organic and inorganic precursors via a modified EISA approach. Because of the well interpenetrated frameworks containing plastic "nano-protector" organic resin polymers and rigid silica "skeleton", ordered mesoporous carbon and silica monoliths with integrated macroscopic morphologies similar to the original composite monoliths are successfully obtained by etching silica in HF solution and simple combustion in air, respectively. The method is simple and reproduceable to prepare cracking-free ordered mesoporous monoliths with a large size ($5 \times 3 \times 0.3$ cm^3) as required. The resultant mesoporous carbon monoliths show a high surface area (~1800 m^2/g) and a large pore volume (~2.65 cm^3/g). Because of the bimodal mesopore size distribution, the mesoporous carbon monoliths show good performances for EDLC with a high capacitance of 186 F/g and good retention (92%) after 1000 cycles. Furthermore, the mesoporous organic−inorganic hybrid monoliths with cracking-free and uniform shape have large potential in optical, catalysis, and electrochemical applications.

■ ASSOCIATED CONTENT

Supporting Information. Nitrogen isotherms and pore size distributions of mesoporous composite, carbon and silica are shown in Figure S1. Cyclic voltammetry curves with a low scan rate and galvanostatic charge/discharge curves with different loading currents of mesoporous carbon monoliths are also shown in this section. This material is available free of charge via the Internet at http://pubs.acs.org/.

■ AUTHOR INFORMATION

Corresponding Author

*E-mail: dyzhao@fudan.edu.cn (D.Z.); botu@fudan.edu.cn (B.T.). Tel: 86-21-51630205. Fax: 86-21-51630307.

■ ACKNOWLEDGMENT

This work was supported by the NSF of China (20890123), the State Key Basic Research Program of the PRC (2009AA033701 and 2009CB930400), Science and Technology Commission of Shanghai Municipality (08DZ2270500), and Shanghai Leading Academic Discipline Project (B108).

■ REFERENCES

(1) Yang, Z. L.; Lu, Y. F.; Yang, Z. Z. *Chem. Commun.* **2009**, *17*, 2270–2277.
(2) Chao, M. C.; Chang, C. H.; Lin, H. P.; Tang, C. Y.; Lin, C. Y. *J. Mater. Sci.* **2009**, *44*, 6453–6462.
(3) Wang, X. N.; Xiong, R. C.; Wei, G. *Surf. Coat. Technol.* **2010**, *204*, 2187–2192.
(4) Zhao, D. Y.; Yang, P. D.; Melosh, N. A.; Feng, J.; Chmelka, B. F.; Stucky, G. D. *Adv. Mater.* **1998**, *10*, 1380–1385.
(5) Hu, J. K.; Shan, W.; Zhang, W. J.; Zhang, Y. H.; Tang, Y. *Microporous Mesoporous Mater.* **2010**, *129*, 210–219.
(6) Nakamura, T.; Yamada, H.; Yamada, Y.; Gurtanyel, A.; Hartmann, S.; Husing, N.; Yano, K. *Langmuir* **2010**, *26*, 2002–2007.
(7) Yu, C. Z.; Tian, B. Z.; Fan, J.; Stucky, G. D.; Zhao, D. Y. *J. Am. Chem. Soc.* **2002**, *124*, 4556–4557.
(8) Yang, P. D.; Zhao, D. Y.; Chmelka, B. F.; Stucky, G. D. *Chem. Mater.* **1998**, *10*, 2033–2036.
(9) Melosh, N. A.; Lipic, P.; Bates, F. S.; Wudl, F.; Stucky, G. D.; Fredrickson, G. H.; Chmelka, B. F. *Macromolecules* **1999**, *32*, 4332–4342.
(10) Nakanishi, K.; Kobayashi, Y.; Amatani, T.; Hirao, K.; Kodaira, T. *Chem. Mater.* **2004**, *16*, 3652–3658.
(11) Zhong, H.; Zhu, G. R.; Wang, P. Y.; Liu, J.; Yang, J.; Yang, Q. H. *J. Chromatogr. A* **2008**, *1190*, 232–240.
(12) Chamieh, J.; Zimmermann, Y.; Boos, A.; Hagege, A. *J. Colloid Interface Sci.* **2009**, *340*, 225–229.
(13) Scott, B. J.; Wirnsberger, G.; Stucky, G. D. *Chem. Mater.* **2001**, *13*, 3140–3150.
(14) Liang, C. D.; Dai, S.; Guiochon, G. *Chem. Commun.* **2002**, *22*, 2680–2681.
(15) Melosh, N. A.; Davidson, P.; Chmelka, B. F. *J. Am. Chem. Soc.* **2000**, *122*, 823–829.
(16) Vasiliev, P. O.; Shen, Z. J.; Hodgkins, R. P.; Bergstrom, L. *Chem. Mater.* **2006**, *18*, 4933–4938.
(17) Xue, C. F.; Wang, J. X.; Tu, B.; Zhao, D. Y. *Chem. Mater.* **2010**, *22*, 494–503.
(18) Melde, B. J.; Holland, B. T.; Blanford, C. F.; Stein, A. *Chem. Mater.* **1999**, *11*, 3302–3308.

(19) Hench, L. L.; West, J. K. *Chem. Rev.* **1990**, *90*, 33–72.
(20) Goltner, C. G.; Henke, S.; Weissenberger, M. C.; Antonietti, M. *Angew. Chem., Int. Ed.* **1998**, *37*, 613–616.
(21) Feng, P. Y.; Bu, X. H.; Stucky, G. D.; Pine, D. J. *J. Am. Chem. Soc.* **2000**, *122*, 994–995.
(22) Yang, H. F.; Shi, Q. H.; Tian, B. Z.; Xie, S. H.; Zhang, F. Q.; Yan, Y.; Tu, B.; Zhao, D. Y. *Chem. Mater.* **2003**, *15*, 536–541.
(23) Clavier, C. W.; Rodman, D. L.; Sinski, J. F.; Allain, L. R.; Im, H. J.; Yang, Y.; Clark, J. C.; Xue, Z. L. *J. Mater. Chem.* **2005**, *15*, 2356–2361.
(24) Si, W. J.; Xing, W.; Zhuo, S. P. *Chin. J. Inorg. Chem.* **2009**, *25*, 1159–1164.
(25) Yang, H. F.; Shi, Q. H.; Liu, X. Y.; Xie, S. H.; Jiang, D. C.; Zhang, F. Q.; Yu, C. Z.; Tu, B.; Zhao, B. *Chem. Commun.* **2002**, *23*, 2842–2843.
(26) Wang, J. C.; Xiang, C. S.; Liu, Q.; Pan, Y. B.; Guo, J. K. *Adv. Funct. Mater.* **2008**, *18*, 2995–3002.
(27) Brun, N.; Prabaharan, S. R. S.; Morcrette, M.; Sanchez, C.; Pecastaings, G.; Derre, A.; Soum, A.; Deleuze, H.; Birot, M.; Backov, R. *Adv. Funct. Mater.* **2009**, *19*, 3136–3145.
(28) Huang, Y.; Cai, H. Q.; Feng, D.; Gu, D.; Deng, Y. H.; Tu, B.; Wang, H. T.; Webley, P.; Zhao, D. Y. *Chem. Commun.* **2008**, *23*, 2641–2643.
(29) Liu, R. L.; Shi, Y. F.; Wan, Y.; Meng, Y.; Zhang, F. Q.; Gu, D.; Chen, Z. X.; Tu, B.; Zhao, D. Y. *J. Am. Chem. Soc.* **2006**, *128*, 11652–11662.
(30) Meng, Y.; Gu, D.; Zhang, F. Q.; Shi, Y. F.; Yang, H. F.; Li, Z.; Yu, C. Z.; Tu, B.; Zhao, D. Y. *Angew. Chem., Int. Ed.* **2005**, *44*, 7053–7059.
(31) Fan, J.; Yu, C. Z.; Wang, L. M.; Tu, B.; Zhao, D. Y.; Sakamoto, Y.; Terasaki, O. *J. Am. Chem. Soc.* **2001**, *123*, 12113–12114.
(32) Scherer, G. W.; Haereid, S.; Nilsen, E.; Einarsrud, M. A. *J. Non-Cryst. Solids* **1996**, *202*, 42–52.
(33) Melosh, N. A.; Davidson, P.; Feng, P.; Pine, D. J.; Chmelka, B. F. *J. Am. Chem. Soc.* **2001**, *123*, 1240–1241.
(34) Qu, D.; Shi, H. *J. Power Sources* **1998**, *74*, 99–107.
(35) Xing, W.; Huang, C. C.; Zhuo, S. P.; Yuan, X.; Wang, G. Q.; Hulicova-Jurcakova, D.; Yan, Z. F.; Lu, G. Q. *Carbon* **2009**, *47*, 1715–1722.